Effect of periodicity and composition in artificial BaTiO_{3}/(Ba,Sr)TiO_{3} superlattices

N. Ortega, A. Kumar, O. A. Maslova, Yu. I. Yuzyuk, J. F. Scott, and R. S. Katiyar

Phys. Rev. B **83**, 144108 — Published 19 April 2011

DOI: 10.1103/PhysRevB.83.144108

Effect of the Periodicity and the Composition in artificial $BaTiO_3$/ $(Ba,Sr)TiO_3$ superlattices

N. Ortega[1], A. Kumar[1*], O.A. Maslova[2], Yu. I. Yuzyuk[2],
J. F. Scott[1,3] and R. S. Katiyar[1*].

[1]Department of Physics and Institute for Functional Nanomaterials, University of Puerto Rico, San Juan, PR 00931-3343 USA
[2]Faculty of Physics, Southern Federal University, Zorge 5, Rostov-on-Don, 344090, Russia
[3]Department of Physics, University of Cambridge, Cambridge CB2 3EQ, UK

ABSTRACT

We have prepared two series of $BaTiO_3/SrTiO_3$ (BT/ST) superlattices (SLs). In the first set, the modulation period (Λ) was varied from 136 Å to 16 Å, whereas in the second set ST was replaced with $Ba_{(1-x)}Sr_xTiO_3$ (BST) ($0<x< 1$) with constant periodicity of ~ 136Å. A total stack height of 10,000 Å (1 μm) was maintained for both the systems. The compositional changes give large spectral changes at x = 40% where the lowest E mode in BT/BST SL became underdamped. X-ray diffraction (XRD) patterns and surface topography of the modulated period revealed a Stranski–Krastanov growth mechanism. The upward frequency shift of the E(1TO) in SLs with decrease in Λ or Ba-concentration in the BST layer was attributed to the in-plane compressive stress induced by the lattice mismatch of the constituent layers. [n.b., here the notation E(1TO) or A_1(2TO) simply designates the vibrational mode of E or A_1 symmetry, with 1TO or 2TO designating the transverse optical branch that is lowest – 1 – or second-lowest – 2– in energy.] In the low frequency region, the folded acoustic phonon (FAP) doublets were observed. Since the low-frequency out-of-plane dielectric constant is directly related to the E(1TO) soft mode frequency, strain engineering in artificial SLs allowed us to modify their

dielectric properties by varying either the Ba/Sr in BST sublayer concentration or the modulation periodicity in the superlattices .

***Electronic mail for correspondence: Ashok Kumar (ashok553@gmail.com); Ram S Katiyar (rkativar@uprrp.edu)**

I. INTRODUCTION

Artificially fabricated superlattices (SLs) constructed by alternate layers of different polar and non-polar perovskites oxides $BaTiO_3$ (BT), $SrTiO_3$ (ST), $LaAlO_3$ and $PbTiO_3$ (PT) have been popular objects of investigations over the past few years [1-10]. In addition to novel physics, SLs exhibit superior properties such as low-loss, high dielectric constant, high polarization, and high Curie temperature that make them attractive for thin-film device applications. Among artificial SLs, different perovskites oxides have been fabricated: ferroelectric/paraelectric BT/ST, $KTaO_3/KNbO_3$, ferroelectric/ferroelectric (BT/PT), paraelectric/paraelectric $LaAlO_3/SrTiO_3$ and ferroelectric/relaxor ($BT/BaTi_{0.68}Zr_{0.32}O_3$). Physical properties different from parent materials can be obtained in the SL structure by modifying the lattice, i.e. change in the unit cell, strain, and the lattice mismatches across the interface between the layers and/or at the film-substrate interface. In case of BT/ST SLs, large stress is induced due to the mismatch between the respective in-plane lattice parameters 3.994/3.905 Å. Local stress in the epitaxial films can be controlled by several ways: varying the deposition conditions, the substrate, varying the film thickness, varying the thickness, or altering the lattice parameters by doping. Stress affects the ionic positions and hence some lattice vibrations (in particular the ferroelectric soft mode which is usually very sensitive to the presence of strain in thin films [11]

The improved properties of these SLs are required for dielectric and ferroelectric device applications such as nonvolatile ferroelectric memories, dynamic random access memory or tunable microwave devices [12,13]. One aspect of SLs is the close relation between structural, electrical properties and morphology. It has been found that the reduction of the thickness of the individual layers in the BT/ST SLs plays a vital role in their functional and structural properties. Visinoiu *et al*. [14-16] reported that the Stranski-Krastanov mechanism governs the growth of BT/ST multilayers, and this feature was attributed to differences in the morphological stability on the growth surfaces. They found BT islands forming on the top of each layer of ST and that the roughness of the top BT layer decreased with increasing number of layers for the same overall thickness.

In this paper our aim is to explore two different approaches: the first is to fabricate SL structures with different modulation periods to investigate the crystal structure and the growth mechanism; the second is to explore the effects of the compositions of one of the constituent layers of the SLs and to investigate the resulting strain and structural properties. We report structural, surface morphology, and Raman characterization of two sets of SLs samples grown on (001) MgO substrates: (1) BT/ST SLs as a function of the modulation period; (2) replacing the ST with $Ba_{(1-x)}Sr_xTiO_3$ (BST) at constant modulation period. Our comparative study revealed peculiarities of structural and lattice-dynamical properties of these two sets of SLs.

II. EXPERIMENTAL

Superlattices of BT/ST and BT/$Ba_{(1-x)}Sr_xTiO_3$ (BT/BST) with x = (0, 0.3, 0.4, 0.5, 0.6, 0.7, 1) were grown on (001) MgO substrate by pulsed laser deposition techniques. The thin-film stack was deposited by alternately focusing the beam on stoichiometric BT, ST, and BST targets. The

films' modulation period (Λ) in $BT_{\Lambda/2}/ST_{\Lambda/2}$ SL was varied between ~16 Å < Λ < 136 Å, while a constant period of Λ= 136 Å was kept in $BT_{\Lambda/2}/BST_{\Lambda/2}$ SLs (see Figure 1). The stacking periodicity $\Lambda/2$ was precisely maintained by controlling the number of laser shots; irrespective of stacking geometry, the total thickness of each SL film was ~10000 Å = 1 μm. Single BT and ST films were deposited under similar deposition conditions as all the SLs, in order to compare them with artificial SLs. An excimer laser (KrF, 248 nm) with a laser energy density of 1.5 J/cm^2 and pulse repetition rate of 10 Hz was used to deposit the SLs. During deposition the substrate was maintained at 830 °C and oxygen pressure at 200 mTorr. The orientation and phase purity of the films were characterized by X-ray diffraction (XRD) using Cu K_α radiation in a Siemens D500 diffractometer. Polarized Raman spectra were recorded in the backscattering geometry using 514.5 nm radiation of an Ar^+ laser and analyzed using a Jobin Yvon T64000 spectrometer equipped with a charge coupled detector (CCD). An optical microscope with 80X objective was used to focus the incident light in a spot of about 2 μm in diameter on the sample. The polarized Raman spectra were obtained in side-view backscattering geometries [17,18]. All Raman spectra in this work were corrected for the Bose-Einstein temperature factor and intensities were normalized. The surface morphology was investigated by atomic force microscopy (AFM) (Veeco) operated in contact mode and using an ultra-sharp silicon tip with a resonance frequency of about 350 kHz. Frequency dependence of the dielectric and ferroelectric properties were measured using an HP4294 impedance analyzer and Radiant tester respectively. For electrical measurements square capacitors were fabricated by dc sputtering with Pt as top electrodes with area of ~10^{-4} cm^2 utilizing a shadow mask. Bottom electrodes were fabricated with conducting $La_{0.67}Sr_{0.33}MnO_3$ on (001) MgO, using PLD technique.

III. RESULTS AND DISCUSSION

A. $BaTiO_3/SrTiO_3$ Superlattices

XRD patterns of BT/ST SLs with different modulation periods are shown in Figure 2. The lattice parameters of ceramic targets used for SLs and substrate are: ST, a = 3.905 Å; BT, c = 4.04 Å, a = 3.99 Å; MgO, a = 4.213 Å. In this work, we have chosen cubic Raman-inactive MgO as a substrate instead of STO substrates even though the lattice mismatch between STO (100) substrate and BT or ST is less compared with MgO single crystal substrate; this was because STO has intense second-order Raman spectra, obscuring the superlattice data. XRD θ-2θ examination revealed the absence of any additional impurity phase, either in single BT and ST films, or in SLs. All films are single-phase and well oriented along the substrate plane. The XRD patterns of SLs contain so-called satellite peaks typical of modulated structures. One central peak located midway between respective BT and ST peaks was observed (see dashed lines in Figure 2), and the satellite peaks are closer for higher order modulation period. The peak positions are given by the Bragg condition [19,20] $\sin\theta_n = n\lambda_x / 2\Lambda$, where n is an integer, and $\lambda_x = 1.5406$ Å is the x-ray wavelength. Therefore, Λ is determined from the position of adjacent peaks: $\Lambda = \lambda_x / 2(\sin\theta_{n+1} - \sin\theta_n)$. The Λ of BT/ST SLs calculated using Bragg equation are in good agreement with that determined by the number of laser shots for SL with $\Lambda \geq 64$. Satellite peaks were not observed for SLs with Λ = 16, 32, and 48 Å in (002) reflection, while weak satellite peaks in (001) reflection were observed for Λ = 32 and 48 Å. The complicated situation arose for Λ = 32, and 48 Å, where the calculated periodicity from Bragg equation gave a 20 Å difference from that based upon the number of laser shots; we interpret this as arising from a non-uniform Stranski–Krastanov (SK) growth mechanism, as reported earlier by Visinoreui *et al*

[21]. This has been attributed to either different growth mechanisms for the two different materials or to a difference in the morphological stability on the growth surfaces caused by the difference of surface energies and different mobilities of Ba and Sr atoms reaching ST and BT layers. Visinoreui *et al* showed the formation of BT islands on top of the ST layer. In order to explain the XRD results, we grew two ultra-thin BT/ST superlattices with only one modulation period: Λ = 48 Å and Λ = 136 Å on MgO with BT on the top of ST. The total thickness of the ultrathin films was 4.8 nm and 13.6 nm respectively. The AFM images of these ultrathin films are showed in Figure 3 (a). The surface topography revealed that the ultra-thin film with Λ = 48 Å has a uniform BT layer in the range of 2-3 nm (see arrows in Figure 3 (a)-left) with dispersive islands (see circles in Figure 3 (a)-left) with height of about 5 nm, resulting in columnar-growth islands based upon the SK mechanism. In case of ultrathin film with Λ = 136 Å, the islands covered almost the entire surface. It indicates that for Λ = 48 Å, individual islands begin to grow; but with increase in the thickness to Λ = 136 Å these islands completely cover the films. This observation suggests the formation of the BT islands on the ST layers based on SK growth mechanism is critical for thickness of $\Lambda \leq$48 Å, where the islands do not coalesce to cover the entire surface of the film. This study explains the difference of periodicity observed in the present study by XRD below 64 Å modulation period and the absence of satellite peaks and folded acoustic phonons for SL with Λ = 32 Å, that is, for SK growth, the layer thickness is ill-defined and non-uniform. This agrees with the direct observation of columnar and SK growth in BT/ST systems by Visinoiu *et al.*

Figure 3(b) shows AFM surface morphology images (1x1 and 3x3 μm^2 x 70-100 nm height) of BT/ST SLs with thickness about 10000 Å having different modulation periods. The

surface roughness of the films with Λ = 16 Å and Λ = 136 Å was estimated to be 3-4 nm depending upon scan area; these high surface roughness values are due to the high deposition temperature of the films. The SL films appeared to be densely packed, smooth, and free of cracks. It was observed that with increase of total film thickness of SL small islands coalesce into larger ones; in plan-view large round islands (grains) were seen in the surface topography of the SL films. Another important observation is the size dependence of the islands with the modulation period. A remarkable increase in the size of islands was observed when the modulation period increased from Λ = 16 Å (Figure 3(b)-left) to Λ = 136 Å (Figure 3(b)-right). This behavior can be explained in terms of the thickness variation of the BT and ST sub-layers in SL thin films. Since we kept a constant overall thickness for all SLs, the thickness of each BT and ST sub-layer decreases with decreasing modulation period. On decreasing the sublayer thickness there is a reduction in the size of the islands. Also with decrease of interlayer thickness there is less time for the small islands to coalescence together to form larger ones. It has shown by Visinoiu et al. [14] in the cross sectional TEM image of BT/ST superlattices that with increase of film thickness the larger islands developed into a column-like structure with bigger islands, as observed in AFM/SEM images.

The ferroelectric soft mode is usually very sensitive to strain in thin films [11,18, 19, 22-24] and so investigation of soft mode behavior in ferroelectric SLs is very useful for better understanding of their physical properties. Figure 4 shows room-temperature polarized Raman spectra of the BT/ST SLs as a function of the modulation period in parallel (Figure 4 (a)) and crossed (Figure 4 (b)) polarizations of the incident and scattering light. Polarized Raman spectra obtained for BT/ST SLs with $\Lambda \geq 64$ Å are very close to those of the single-domain BT crystal [17], and all the peaks can be identified (see Ref. 23 for details). The parallel polarized

($Y(ZZ)\overline{Y}$ geometry) spectra contain longitudinal (LO) and transverse (TO) A_1 optical modes, whereas crossed polarized ($Y(ZX)\overline{Y}$ geometry) spectra showed mainly E(LO) and E(TO) modes. However, symmetry-forbidden scattering from the higher-energy totally-symmetric modes A_1(2TO) and A_1(3TO) was observed. Therefore these polarization-dependent Raman spectra exclude tetragonal symmetry of the SLs with the *c*- axis being normal to the substrate. The appearance of the A_1 modes in the crossed-polarized geometries implies symmetry lowering to orthorhombic or monoclinic. Raman selection rules can be relaxed due to the presence of a-domains and corresponding domain walls. Actually, partial depolarization of incident/scattered light may be a reason of the "leak" of A1 modes into forbidden geometries. In our case intensity of A1 modes in crossed polarized spectra is too high to speak about their leakage. The most significant difference with respect to pure BT and ST thin films was observed in crossed polarized spectra (Figure 4 (b)) where the E(TO) component of the soft mode is markedly altered from the bulk value of the BT crystal. Such differences in Raman spectra have been reported in PT/BT ferroelectric SLs [19] and BT/$BaTi_{0.68}Zr_{0.32}O_3$ ferroelectric/relaxor SLs [20] and attributed to the effect of internal stress. We note that these particular selection rule violations can also arise from homogeneous stress and do not require inhomogeneous stress gradients (flexoelectricity) [13]. The dependence of the peak positions of E(1TO) and A_1(2TO) modes with modulation period was observed in BT/ST SLs (see dashed lines in Figure 4). The frequency of the E(1TO) soft mode increases with decreasing the modulated period from 115 cm^{-1} (Λ = 136 Å) to 124 cm^{-1} (Λ = 64 Å). We already reported [11, 22,23,25] that a significant shift of the E(TO) soft mode can be observed due to two-dimensional 2D stress imposed by the substrate; however, in the case of BT/ST SL grown on MgO the upward shift of the soft mode

and the broadening of the modes in BT sublayers can be enhanced due to the internal in-plane 2D compressive stress caused by the lattice mismatch between BT and ST layers. Extensive studies on $Ba_{0.7}Sr_{0.3}TiO_3$ (BST70) thin films of different thickness grown on MgO substrate by our group suggest a remarkable downward shift of the E(TO) soft mode with decrease in the thickness of the thin films below 400 nm [25]. However this stress becomes fully relaxed (i.e. no change in the E(TO) soft mode position was observed) above 400 nm film thickness. Since all samples have the same total thickness and were fabricated under the same conditions, the effective stress is only to interlayer constituents, not by the substrate interface. The hardening of the soft mode in single ST thin films compared to bulk crystal values was observed and explained by Sirenko *et al.* [26]. It is worth mentioning that the hardening of the E(TO) soft mode in the BT/ST SLs (for $\Lambda > 64$ Å) is much more significant with respect to single films of BT, ST or BST.

When the modulation period decreases ($\Lambda < 64$ Å), the peaks in diagonal-polarizability tensor-component spectra exhibit broadening, and the interference dip at ~160 cm^{-1} is very weak. The peak position of the A_1(2TO) mode in this parallel-polarized spectra moves to lower wave numbers with decreasing Λ from 278 cm^{-1}(Λ= 136 Å) to 249 cm^{-1} (Λ= 64 Å) as one can see in dashed line in Figure 4 (a). The peak corresponding to A_1(3TO) mode acquires a high-frequency shoulder. Also, from Figure 4 (b), in SLs with $\Lambda < 64$ Å the E(1TO) mode becomes very broad and the exact frequency determination of this mode is not possible. The downward frequency shift and broadening are typical for poorly ordered systems; therefore our Raman spectroscopy suggests the formation of BT-ST solid solutions at the interfaces of the very thin layers when $\Lambda <$ 64 Å. This conclusion is in agreement with the XRD data, where poor resolution of satellite peaks was observed.

Figure 4 (c) shows the low-frequency region where the activation of folded acoustic phonon (FAP) doublets was observed. This doublet appears due to the new artificial periodicity imposed by the superlattice structure [27]. Due to new periodicity, the Brillouin zone is folded into the new SL Brillouin zone. In a superlattice of n unit cells repeat distance, the lowest frequency phonons observable via Raman spectroscopy should arise from the acoustic phonon branch at $q = q_o/n$, where $q_o = \pi/a$ in the case of a simple cubic perovskite, and a is the lattice constant. In other words, $q = \pi/na = \pi/\Lambda$. Hence in the case of Λ= 136 Å, we have n =34 and the acoustic phonon can be described as occurring at q =0.029 [00ζ] in the single-cell Brillouin zone. According to that, the wave number of FAP increases with decreasing the modulation period (Λ) of BT/ST SL. However FAP were not observed in the samples with Λ< 64 Å. That means the observation of the FAP is an additional signature of the formation of SL structure.

B. $BaTiO_3/Ba_{(1-x)}Sr_xTiO_3$ Superlattices

Lattice parameters of solid solutions BST systematically decreases with increasing Sr content, and almost exactly follows a linear Vegard's law [28]. In order to get further information concerning the role of interlayer strain, we analyzed the SLs with partial replacement of Sr by Ba. BST layers are used to build up internal stain by varying the value of the lattice in the plane of interface layers where a = 3.905 Å typical for ST, and a = 3.990 Å typical for BT. A series of specimens where ST layer was replaced by BST with variable Ba/Sr concentrations were investigated for this purpose. Interlayer strain can be minimized by making Ba-rich BST sublayers while situation can be reversed (maximal strain) with Sr-rich BST sublayers.

Figure 5 (a) and (b) show the XRD of BT/BST SLs of (001) and (002) diffraction peaks respectively, with variable Ba/Sr content and fixed modulation period (Λ= 136 Å). The notations we use in the figures for BT/BST SLs, correspond to different percentage composition of the BST sublayer, which is Ba/Sr: 0/100, 30/70, 40/60, 50/50, 60/40, 70/30, 100/0, where 0/100 correspond to BT/ST SL and 100/0 to pure BT film. It is evident that there is variation of the position in the satellite reflections due to variation of the layers. In fact, lattice parameters of BST sublayers inside BT/BST SLs depend on the Ba/Sr content. According to Le Marrec *et al.* [19] the X-ray results can be interpreted as diffraction from entire superlattice structure ($BT_{\Lambda/2}$ /$BST_{\Lambda/2}$) where the unit cell of the SL has a period Λ. This effect was clearly seen in both sets of SLs, while the central peak was at the same position in BT/ST SLs (Λ > 48 Å) (see dashed lines in the Figure 2 (a) and (b)). In case of BT/BST SLs, the central peak moved toward ST position peak when decreasing Ba concentration in BST sublayer (see dashed lines in the Figure 5 (a) and (b)). Also, the XRD results show similar SL structural properties either by increasing the modulation period in BT/ST SLs or by variation of the composition of BST sublayer (x= 0 - 1) in BT/BST SLs at constant Λ = 136 Å. As expected, no significant change in the islands size in AFM image (see Figure 3(c)) was observed for BT/BST SLs, which has constant modulation period (Λ = 136 Å).

Figure 6 shows room-temperature polarized Raman spectra of BT single phase thin film and BT/BST SLs with a constant modulation period Λ = 136 Å. The parallel-polarized (Figure 6 (a)) and crossed-polarized (Figure 6 (b)) spectra of BT/BST SLs show main characteristics that were observed in BT/ST SLs, but in this case the composition of BST sublayer was varied instead of the modulation period. It is worth mentioned that presence of A_1 (2TO) and A_1(3TO)

lines in the $Y(ZX)\overline{Y}$ Raman spectrum of single thin film of BT excludes the tetragonal *c*-domain structure and more likely the BT film in either monoclinic (*r* phase) or orthorhombic (*aa*-phase) as was predicted by first-principle and phenomenological calculations for epitaxial perovskites on cubic substrates [29,30]. Raman spectra of all BT/BST SLs also contain similar totally-symmetric modes and all these SLs are, therefore, monoclinic or orthorhombic. In the parallel-polarized $Y(ZZ)\overline{Y}$ spectra, we observed an abrupt frequency shift of the A_1(2TO) peak from 261 cm^{-1} to 271 cm^{-1} when Ba/Sr composition content changed from 50/50 to 40/60 in the BST sublayer (see dashed line in Figure 6 (a)). Perry and Hall *et al*. [31] have studied Raman spectra of $BaTiO_3$ single crystal as a function of temperature. They have seen abrupt shift of the peak near 250 cm^{-1} at the tetragonal-orthorhombic and orthorhombic-rhombohedral phase transitions. At these transitions the direction of the polarization changes. In our case the shift is not so large and can be attributed to the change of the polarization angle in the orthorhombic or monoclinic phase of the SL. When we cross the 50/50 concentration in BST layer we are in the Sr-rich side and lattice mismatch between BT and BST layers increases. Probably interlayer coupling induces larger 2D stress. Note that below 50/50 E(TO) soft mode is underdamped and also markedly upshifted.

The frequency of the E(1TO) soft mode in the crossed-polarized $Y(ZX)\overline{Y}$ spectra increased from 35 cm^{-1} to 115 cm^{-1} when Ba concentration in the BST sublayers changed from 100 to 0. As in pure BT crystals this mode is also overdamped in BT film with the fitted frequency being ~35 cm^{-1} [32]. In BT/BST (Ba/Sr:70/30) SL the lattice mismatch between the sublayers is small, the overdamped character of the E(1TO) soft mode is preserved, but its frequency is shifted up to ~58 cm^{-1}. Further increase of Sr content (above 40%) in the BST

sublayers changes drastically the width of the E(1TO) soft mode, and underdamped peaks are observed in all other SLs. Using a conventional fitting procedure, we found the dependence of the E(1TO) frequency as a function of Ba/Sr content in BST sublayers (Figure 7). Actually, the position of the E(TO) soft mode and the related values of the dielectric constant can be obtained by varying Ba/Sr concentration in BST sublayers. These results support the idea that the upward shift of the soft modes in the SL is due to the internal stress induced by the lattice mismatch between the constitutive sublayers. The stress between BT and BST layers is modified due to the change in lattice parameters of the BST layers caused by the variation of the Ba/Sr content.

Figure 6 (c) shows dependence of the FAP as a function of the BST composition in BT/BST SLs. Although the modulation period was kept constant (Λ= 136 Å), a small variation of the FAP doublets was observed because the sound velocity depends on the Ba/Sr ratio. Note that FAP were not observed in the BT/BST (Ba/Sr:70/30) SL in which the E(1TO) soft mode is overdamped, BT/BST (Ba/Sr:70/30) SL is overlapped with the overdamped soft mode in $Y(ZX)\overline{Y}$ geometry and cannot be properly detected because intensity of FA phonon is very weak with respect to the overdamped soft mode. Probably, FAP are either overlapped or beyond the detection of Raman spectroscopy for this particular concentration (because lattice parameters are very close in the case of these layers).

SLs sometimes have unusual functional properties compared to their parent material, [6, 7, 10]. Although the main focus of this article is to report and analyze the crystal structure, phonon anomalies, and their correlation with growth mechanisms, we have done room temperature dielectric and ferroelectric characterization of one of the SLs: BT/$Ba_{0.3}Sr_{0.7}TiO_3$ (BT/BST3070) with a constant modulation period (Λ = 136 Å) with 1 μm total film thickness.

The frequency dependence of the dielectric constant and loss tangent (Figure 8(a)) show almost constant high values of dielectric constant (~1300) below 10 kHz and relatively low loss tangent (< 0.1) at frequencies below 10 kHz. Strong polarization switching with well saturated hysteresis was observed in BT/BST(30/70) (Figure 8(b)) at different frequencies. However, characteristically asymmetric (imprint) behavior of the ferroelectric loop was also observed. Similar behavior in polarization loops was observed by Lee et al. in case of three-component ferroelectric SLs [33]. The imprint may be due to several reasons: (i) different work function of the dissimilar top and bottom electrodes (Pt and $La_{0.67}Sr_{0.33}MnO_3$); (ii) development of built-in internal stress across the interlayers; and (iii) compositionally broken inversion symmetry with the creation of new lattices in the SLs [34]. It is worth mentioning that the magnitude of ferroelectric polarization obtained in case of BT/BST(30/70) SL which containing ferroelectric and paraelectric components is comparable to BT thin films on different substrates [35,36].

IV. CONCLUSIONS

We have prepared a series of BT/ST SLs with different periodicity and BT/$Ba_{(1-x)}Sr_xTiO_3$ SLs with fixed periodicity but different Sr/Ba compositions. The XRD and surface topography studies on BT/ST SLs revealed that below a critical periodicity (Λ< 64 Å) the growth mechanism is Stranski-Krastanov with a 20 Å difference in observed values and those predicted from deposition parameters. Raman spectroscopy suggests the formation of BT-ST solid solutions at the interfaces of the very thin constitutive layers. Raman scattering studies of BT/ST SLs with $\Lambda \geq$ 64 Å revealed hardening of the E(1TO) soft mode due to the internal in-plane [2D] compressive stress caused by the lattice mismatch between BT and ST layers. The folded acoustic phonon doublets were observed due to the new artificial periodicity only in SLs with Λ

≥ 64 Å, while their absence in the SLs below the critical periodicity correlates with the absence of XRD satellite peaks and implies non-uniform layers. Raman study of BT/BST SLs with a constant modulation period Λ = 136 Å revealed significant frequency variation of the E(1TO) soft mode from 115 to 35 cm^{-1} when Ba concentration in BST sublayers was changed from 0 to 100. Since the low-frequency dielectric constant is directly related to the E(1TO) soft mode frequency, strain engineering in artificial SLs allows us to modify their dielectric properties by varying Ba/Sr concentration in BST sublayers.

REFERENCES

[1]H. Tabata, H. Tanaka, and T. Kawai, Appl. Phys. Lett. 65, 1970 (1994).

[2]J.B. Neaton and K.M. Rabe. Appl. Phys. Lett. 82, 1586 (2003).

[3]A. I. Lebedev, Phys. Sol. St. 51, 2324 (2009).

[4]H. Chaib, A. Khalal, and A. Nafidi. Ferroelectrics. 386, 41 (2009).

[5]M. Sepliarsky, S.R. Phillpot, D. Wolf, M. G. Stachiotti, and R.L. Migoni. J. Appl. Phys. 90, 4509 (2001); Phys. Rev. B. 64, 060101(R) (2001).

[6] E. Bousquet, M. Dawber, N. Stucki, C. Lichtensteiger, P. Hermet, S. Gariglio, J.M. Triscone and P. Ghosez. Nature. 452, 732 (2008).

[7] M. Dawber, N. Stucki, C. Lichtensteiger,. S. Gariglio, P. Ghosez, J.M. Triscone. Adv. Mater. 19, 4153 (2007).

[8] V.R. Cooper, and K.M. Rabe. Phys. Rev. B. 79, 180101(R) (2009); V. R. Cooper, K. Johnston and K.M. Rabe, Phys. Rev. B 76, 020103 (2007).

[9] K.H. Chew, M. Iwata, and F.G. Shin. Ferroelec. Lett. 36, 12 (2009).

[10]D.A. Tenne, A. Bruchhausen, N.D. Lanzillotti-Kimura, A. Fainstein, R.S. Katiyar, A. Cantarero, A. Soukiassian, V. Vaithyanathan, J. H. Haeni, W. Tian, D.G. Schlom, K.J. Choi, D. M. Kim, C.B. Eom, H. P. Sun, X.Q. Pan, Y.L. Li, L. Q. Chen, Q.X. Jia, S. M. Nakhmanson, K. M. Rabe, X.X. Xi. Science. 313, 1614 (2006).

[11]Y.I Yuzyuk, R.S. Katiyar, V.A. Alyoshin, I.N. Zakharchenko, D.A. Markov, and E.V. Sviridov. Phys. Rev. B. 68, 104104 (2003).

[12] M. Dawer, K.M. Rabe, and J. F. Scott. Rev. Mod. Phys. 77, 108-130 (2005).

[13] J. F. Scott, J. Chem. Phys. 48, 874 (1968).

[14]A. Visinoiu, R. Scholz, S. Chattopadhyay, M. Alexe, and D. Hesse. Jpn. J. Appl. Phys. 41, 6633 (2002)

[15]A. Visinoui, R. Scholz, M. Alexe, and D. Hesse. Appl. Phys. A. 80, 229 (2005).

[16]A. Visinoui, R. Scholz, M. Alexe, and D. Hesse. Mat. Res. Soc. Symp. Proc. 748, U13.2.1 (2003).

[17]M. DiDomenico, S.H. Wemple (Jr.), and P.S. Porto. Phys. Rev. 174, 522 (1968).

[18]Yu.I. Yuzyuk, A. Almeida, M.R. Chaves, V.A. Alyoshin, I.N. Zakharchenko, and E.V. Sviridov, Phys. Status Solidi B 222, 535 (2000).

[19]F.L. Marrec, R. Farhi, M.E. Marssi, J.L. Dellis, G. Karkut, and D. Ariosa. Phys. Rev. B. 61, R6447 (2000).

[20]F.D. Guerville, M.E. Marssi, I.P. Raevski,M.G. Karkut and Y.I. Yuzyuk. Phys. Rev. B. 74, 064107 (2006).

[21]A. Visinoui, R. Scholz, S. Chattopadhyay, M. Alexe, and D. Hesse. Jpn. J. Appl. Phys. 41, 6633 (2002)

[22]Yu. I. Yuzyuk, V.A. Alyoshin, I.N. Zakharchenko, E.V. Sviridov, A. Almeida, and M.R. Chaves**.** Phys. Rev. B. 65, 134107 (2002).

[23]Rasmi R. Das, Yu. I. Yuzyuk, P. Bhattacharya, V. Gupta, and R.S. Katiyar. Phys. Rev. B. 69, 132302 (2004).

[24]H. Bouyanfif, El. Marssi, N. Lemée, F. Le. Marrec, M.G. Karkut, and B. Phys. Rev. B. 71, 020103 (2005).

[25] R.S. Katiyar, Yu. I. Yuzyuk. Vibrational spectroscopy 45, 108-111 (2007).

[26]A. A. Sirenko, C. Bernhard, A. Golnik, Anna M. Clark, Jianhua Hao, Weidong Si, and X. X. Xi, Nature 404, 373, (2000).

[27]B. Jusserand and M. Cardona. "Raman spectroscopy of vibrations in Superlattices" Light Scattering in solids V: Superlattices and other Microstructures. (Topics in Applied Physics vol. 66) edited by M. Cardona and Grüntherodt G. Springer, Heidelberg pp. 49-152, (1989).

[28]V.V. Lemanov, E.P. Smirnova, P.P. Syrnikov, and E.A. Tarakanov. Phys. Rev. B. 54, 3151 (1996).

[29]O. Diéguez, K. M. Rabe, and D. Vanderbilt, Phys. Rev. B 72, 144101 (2005).

[30]V. B. Shirokov, Yu. I. Yuzyuk, B. Dkhil, and V. V. Lemanov, Phys. Rev. B 75, 224116 (2007).

[31]C. H. Perry and D. B. Hall, Phys. Rev, Lett. 15, 700 (1965).

[32]A. Scalabrin, A.S. Chaves, D.S. Shim, and S.P.S. Porto. Phys. Status Solidi B 79, 731 (1977).

[33]H. N. Lee, H. M. Christen, M. F. Chisholm, Ch. M. Rouleau and D. H. Lowndes. Nature, 433, 395 (2005).

[34]N. Sai, B. Meyer, and D. Vanderbilt. Phys. Rev. Lett. 84, 5636 (2000).

[35] L. Qiao and X. Bi, Appl. Phys. Lett. 92, 062912 □2008.

[36] Q. X. Jia, L. H. Chang, and W. A. Anderson, Thin Solid Films 259,264 (1995).

FIGURE CAPTIONS

Figure 1. A sketch diagram of the (a) BT/ST and (b) BT/BST SLs thin films.

Figure 2. X-ray diffraction patterns of single BT and ST films and BT/ST SLs with modulation period (Λ) varied from ~ 16 to 136 Å: (a) (001) and (b) (002) peaks.

Figure 3. (a) AFM images of ultra-thin BT/ST film with a area of 0.5 x 0.5 μm^2 of modulation periods of Λ= 48 Å and 136 Å with thickness about 4.8 nm and 13.6 nm respectively. AFM topography images with a area of 3 x 3 μm^2 and 1 x 1 μm^2 (insets) of: (b) BT/ST SLs grown with different modulation period (Λ= 16 Å, 120 Å), (c) BT/BST SLs with variable composition (%) of Ba/Sr in BST layers (30/70, 50/50). The total thickness of the films was kept constant (~10000 Å).

Figure 4. Polarized Raman spectra in (a) parallel and (b) crossed scatering geometries for BT/ST SLs for different modulation period Λ = 16 to 136 Å. (c) Folded acoustic phonons of BT/ST SLs. All spectra were measured at room temperature. Dotted lines show softening of phonons.

Figure 5. X-ray diffraction patterns of Single BT and ST films and BT/BST SLs with Ba content varying from 0 to 100% in BST layer, with a constant modulation period (Λ = 136 Å). (a) (001) and (b) (002) peaks.

Figure 6. Polarized Raman spectra in (a) parallel and (b) crossed scatering geometries for BT single thin film and BT/BST SLs with Ba content varying from 0 to 100%, in BST layer with a constant modulation period (Λ = 136 Å). (c) Folded acoustic phonons of BT/BST SLs. All spectra were measured at room temperature. Dotted lines show softening of phonons.

Figure 7. Frequency (υ) of the E(1TO) soft mode as a function of Ba/Sr (%) content in BST layer of BT/BST SLs.

Figure 8. (a) Frequency dependence of (a) the dielectric constant and the loss tangent and (b) ferroelectric hysteresis loop of BT/$Ba_{0.3}Sr_{0.7}TiO_3$ SL with a constant modulation period (Λ = 136 Å). Total thickness of the films was ~10000 Å.

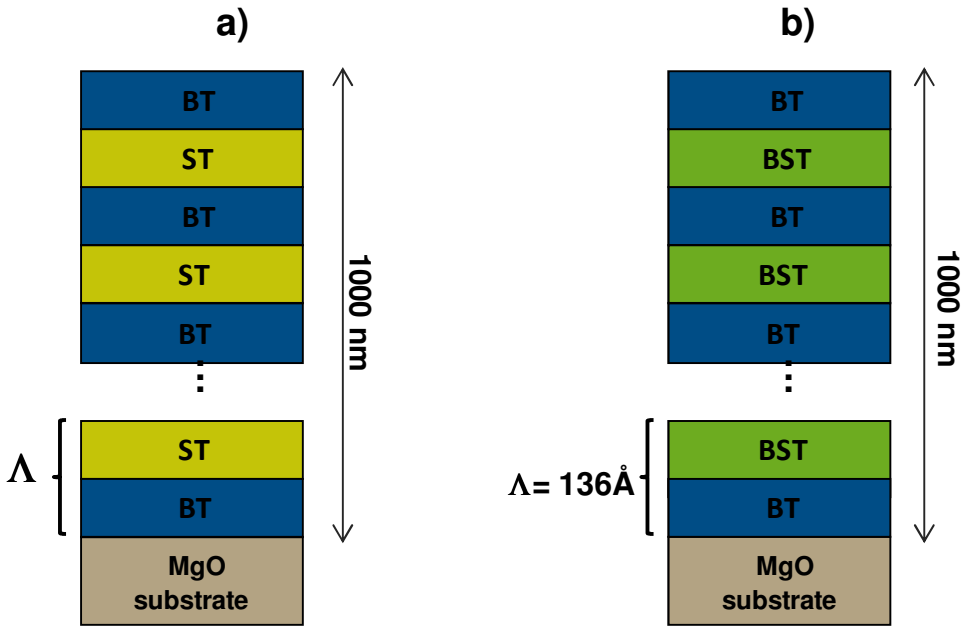
a)
BT
ST
BT
ST
BT
1000 nm
Λ
ST
BT
MgO
substrate
b)
BT
BST
BT
BST
BT
1000 nm
Λ= 136Å
BST
BT
MgO
substrate

Figure 1

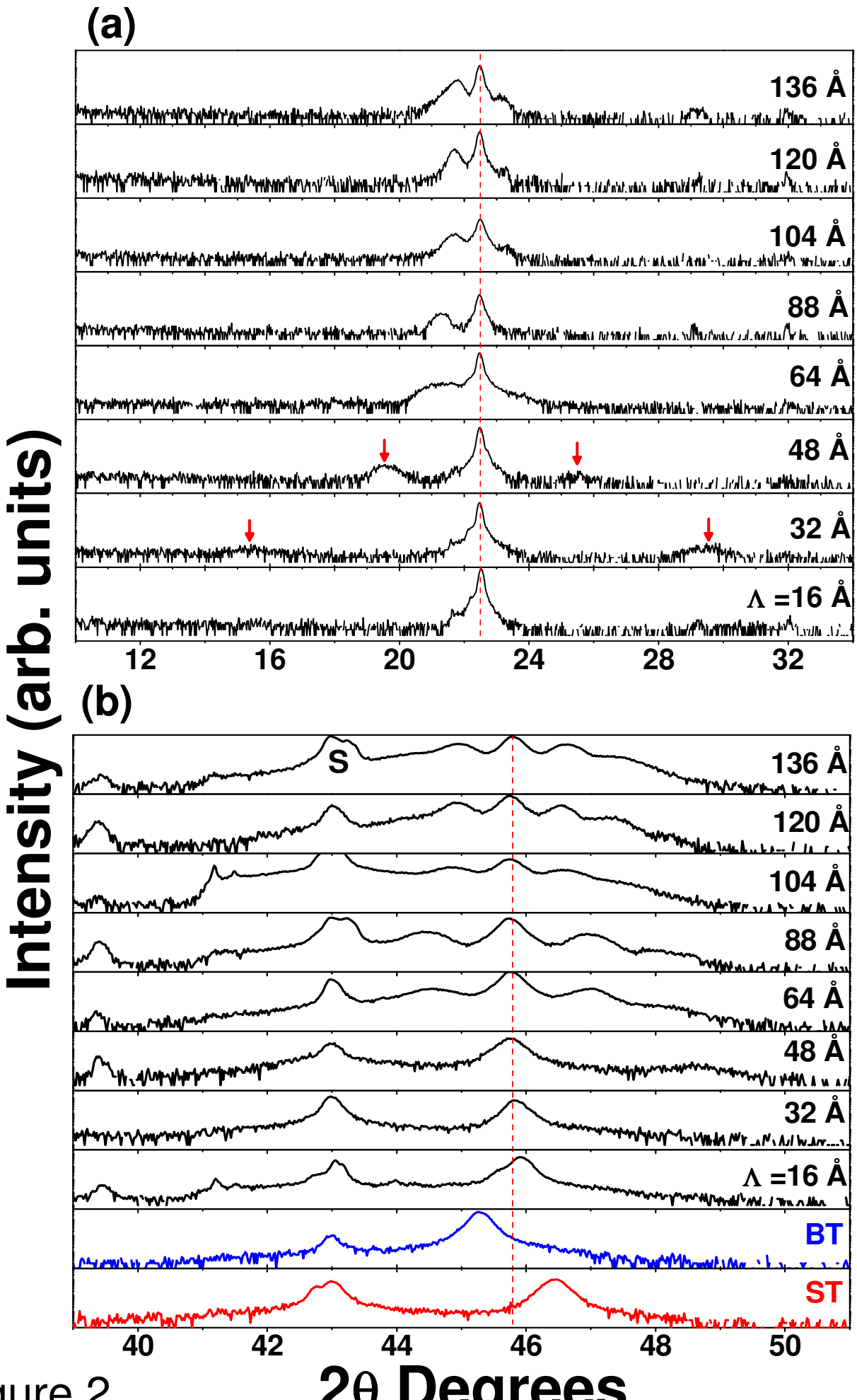
(a)
136 Å
120 Å
104 Å
88 Å
64 Å
48 Å
32 Å
Λ =16 Å
12
16
20
24
28
32
(b)
S
136 Å
120 Å
104 Å
88 Å
64 Å
48 Å
32 Å
Λ =16 Å
BT
ST
40
42
44
46
48
50
Intensity (arb. units)
2θ Degrees

Figure 2.

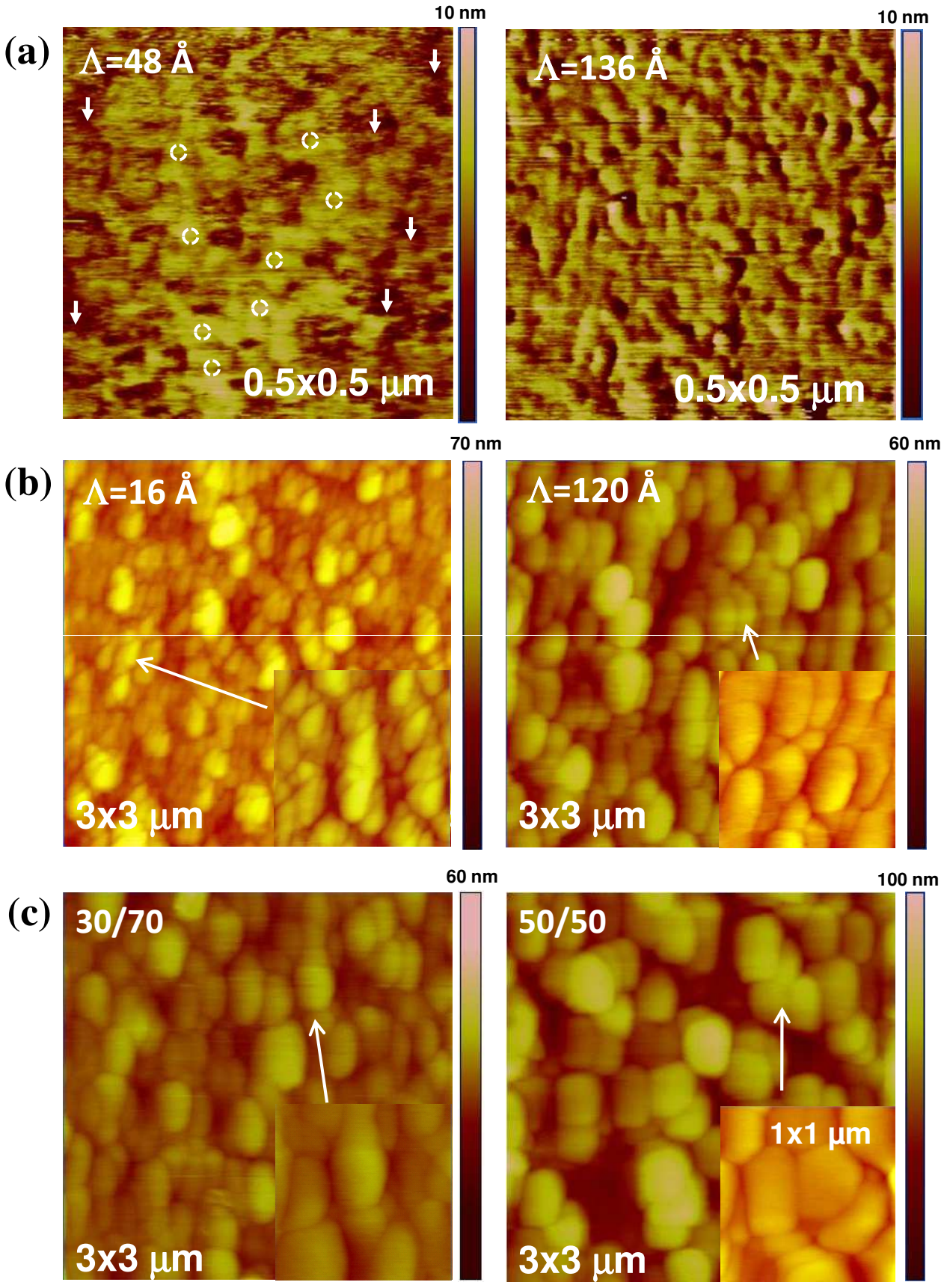
(a)
Λ=48 Å
0.5x0.5 μm
10 nm
Λ=136 Å
0.5x0.5 μm
10 nm
(b)
Λ=16 Å
3x3 μm
70 nm
Λ=120 Å
3x3 μm
60 nm
(c)
30/70
3x3 μm
60 nm
50/50
1x1 μm
3x3 μm
100 nm

Figure 3

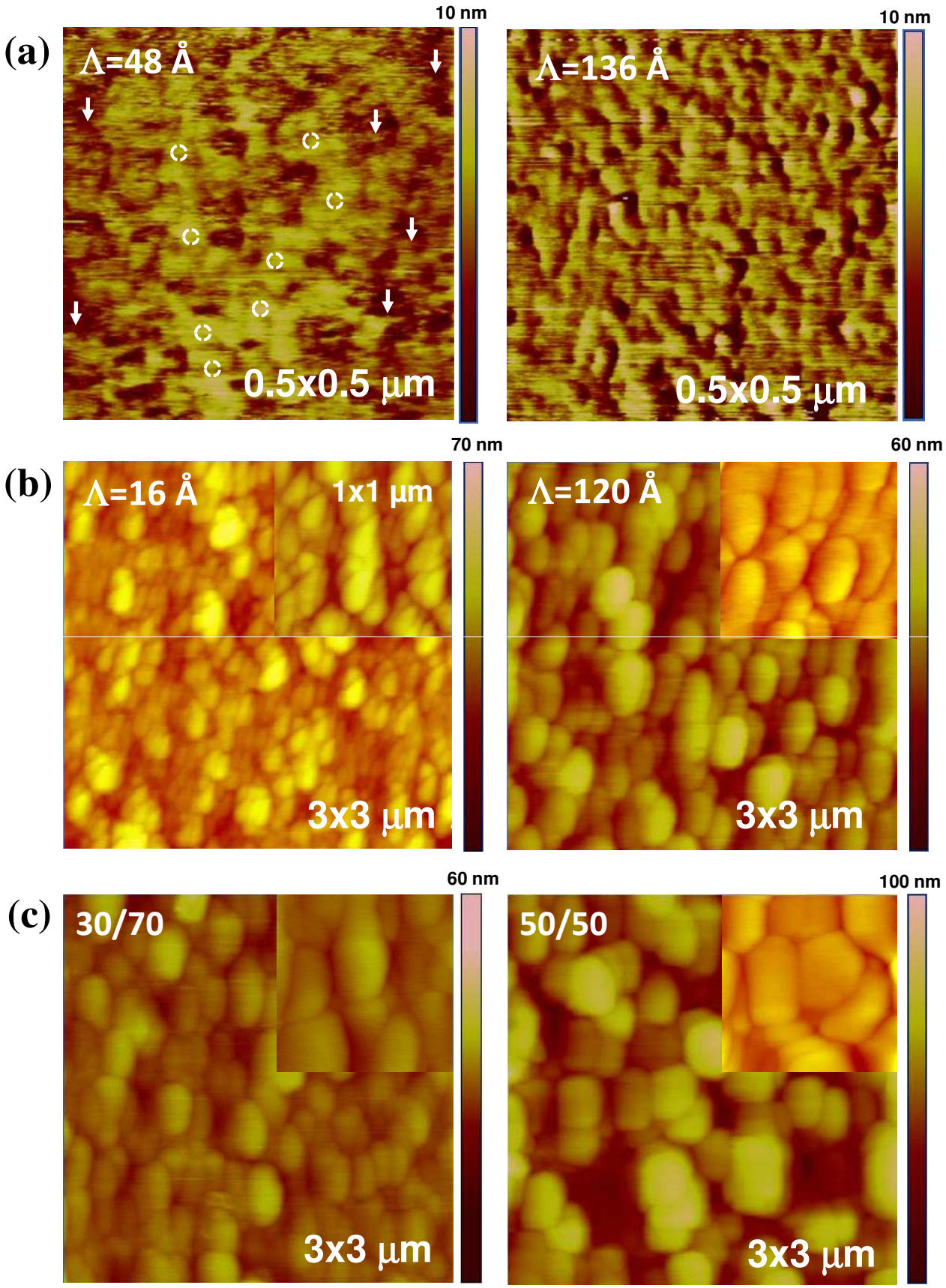
(a)
Λ=48 Å
0.5x0.5 μm
10 nm
Λ=136 Å
0.5x0.5 μm
10 nm
(b)
Λ=16 Å
1x1 μm
3x3 μm
70 nm
Λ=120 Å
3x3 μm
60 nm
(c)
30/70
3x3 μm
60 nm
50/50
3x3 μm
100 nm

Figure 3

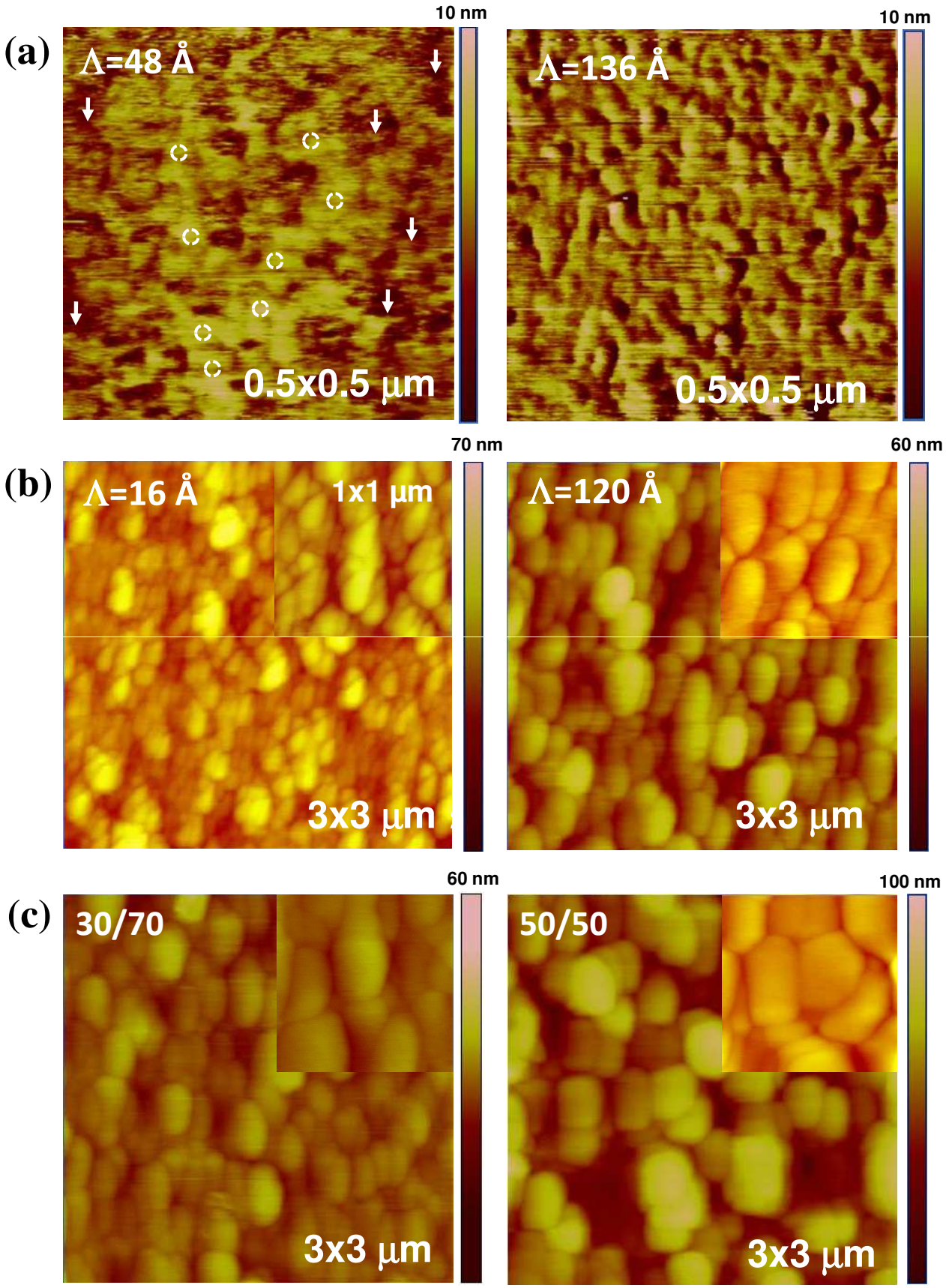
(a)
Λ=48 Å
0.5x0.5 μm
10 nm
Λ=136 Å
0.5x0.5 μm
10 nm
(b)
Λ=16 Å
1x1 μm
3x3 μm
70 nm
Λ=120 Å
3x3 μm
60 nm
(c)
30/70
3x3 μm
60 nm
50/50
3x3 μm
100 nm

Figure 3

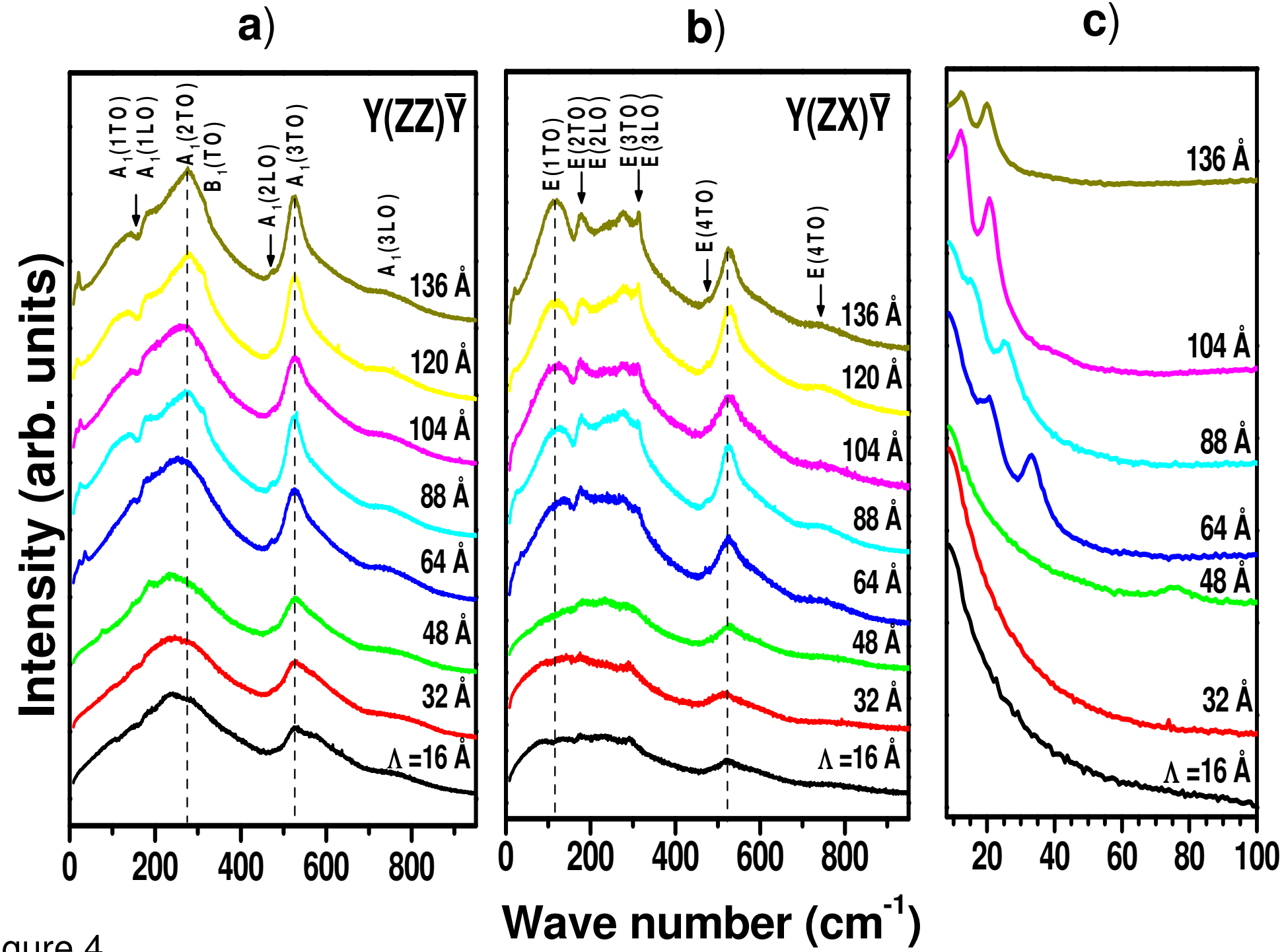
a)
b)
c)
Y(ZZ)Ȳ
Y(ZX)Ȳ
A1(1TO)
A1(1LO)
A1(2TO)
B1(TO)
A1(2LO)
A1(3TO)
A1(3LO)
E(1TO)
E{2TO}
E{2LO}
E{3TO}
E{3LO}
E(4TO)
E(4TO)
136 Å
120 Å
104 Å
88 Å
64 Å
48 Å
32 Å
Λ =16 Å
Intensity (arb. units)
Wave number (cm-1)
0
200
400
600
800
20
40
60
80
100

Figure 4.

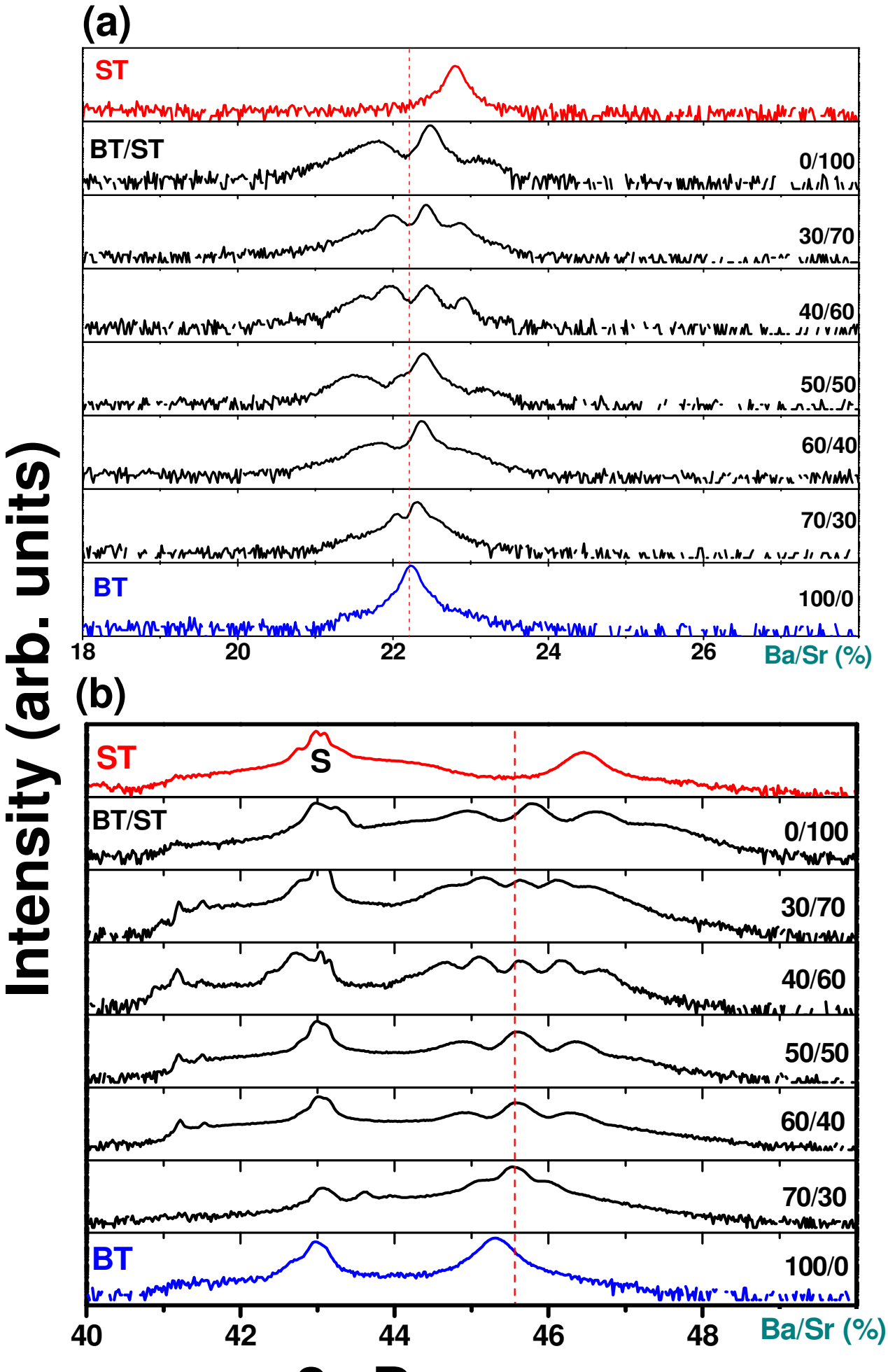
(a)
ST
BT/ST
0/100
30/70
40/60
50/50
60/40
70/30
BT
100/0
18
20
22
24
26
Ba/Sr (%)
(b)
ST
S
BT/ST
0/100
30/70
40/60
50/50
60/40
70/30
BT
100/0
40
42
44
46
48
Ba/Sr (%)
Intensity (arb. units)
2θ Degrees

Figure 5

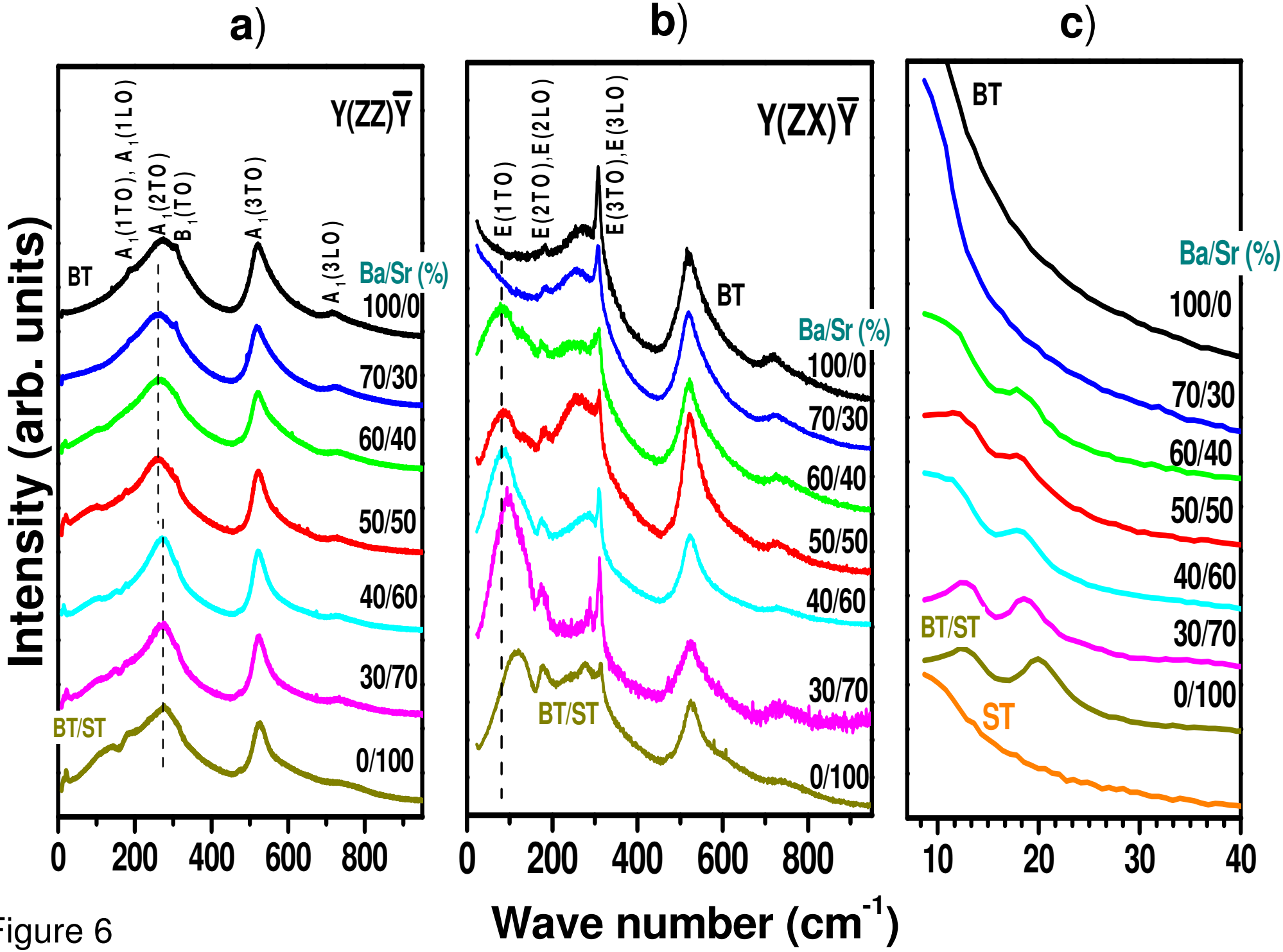
a)
b)
c)
Y(ZZ)Ȳ
Y(ZX)Ȳ
A1(1TO), A1(1LO)
A1(2TO)
B1(TO)
A1(3TO)
A1(3LO)
E(1TO)
E(2TO),E(2LO)
E(3TO),E(3LO)
BT
BT/ST
ST
Ba/Sr (%)
100/0
70/30
60/40
50/50
40/60
30/70
0/100
Intensity (arb. units)
Wave number (cm-1)
0
200
400
600
800
10
20
30
40

Figure 6

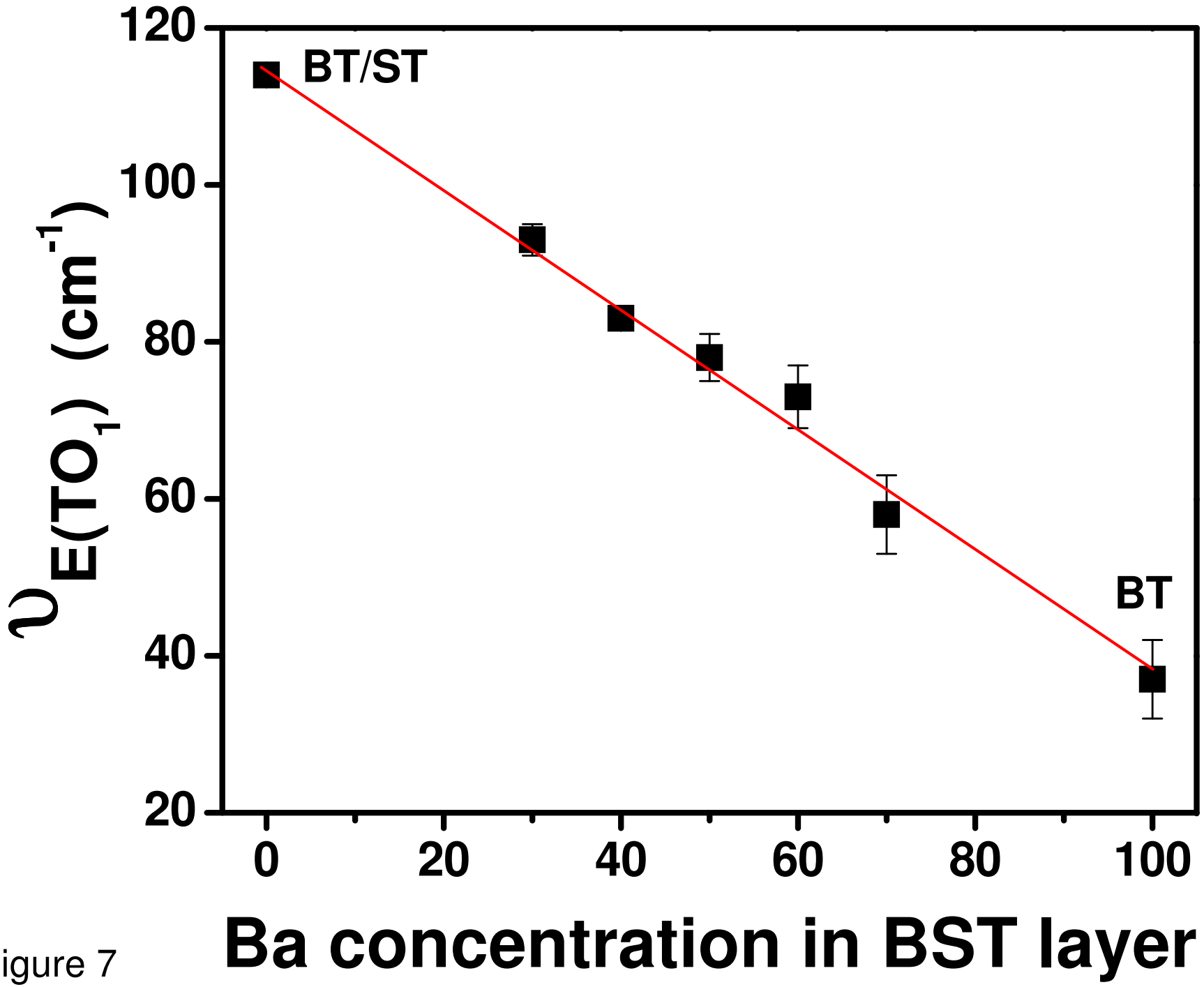
120
100
80
60
40
20
0
20
40
60
80
100
BT/ST
BT
$\upsilon_{E(TO_1)}$ (cm^{-1})
Ba concentration in BST layer

Figure 7

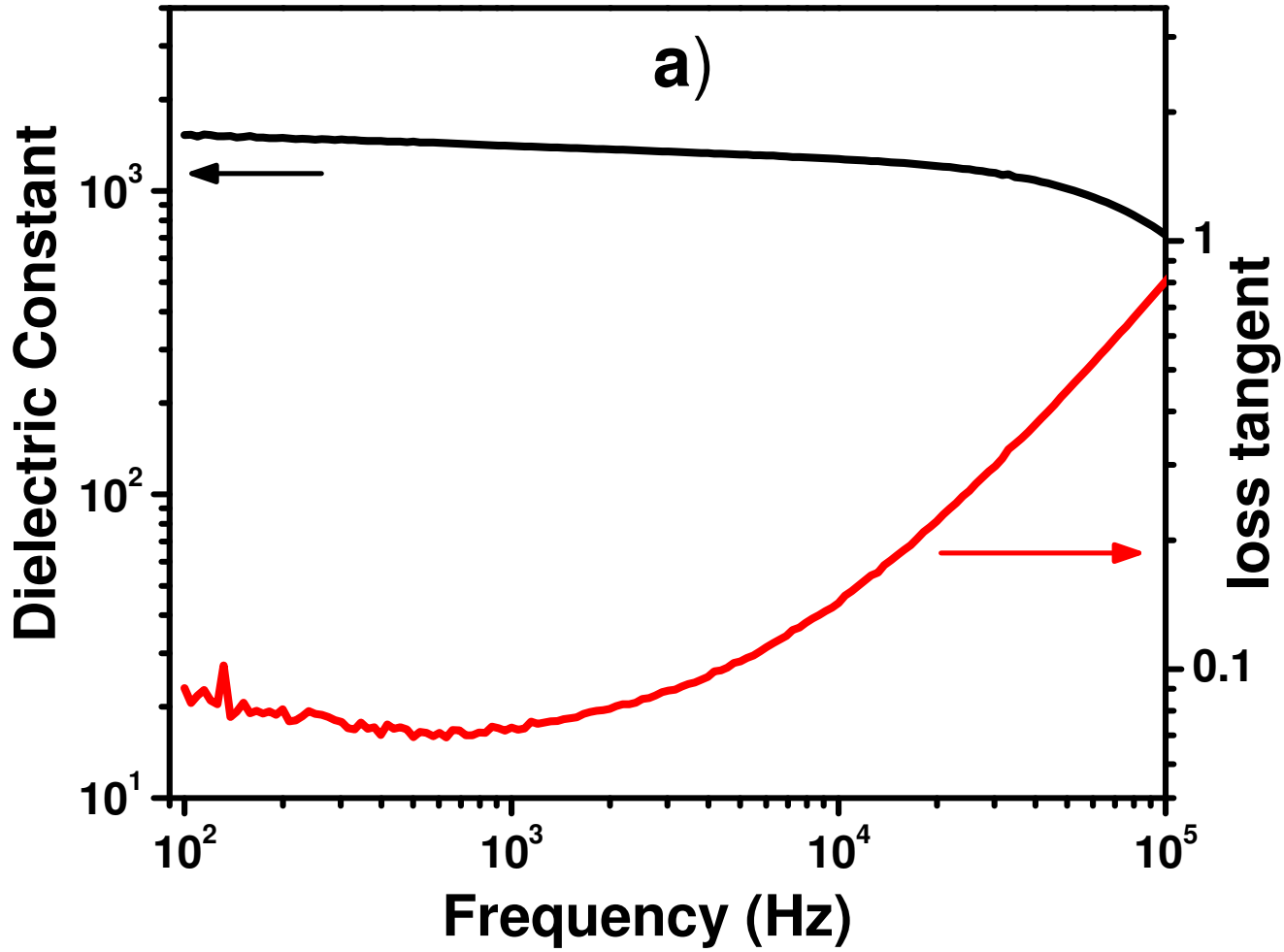
a)
Dielectric Constant
loss tangent
Frequency (Hz)
10^1
10^2
10^3
1
0.1
10^2
10^3
10^4
10^5

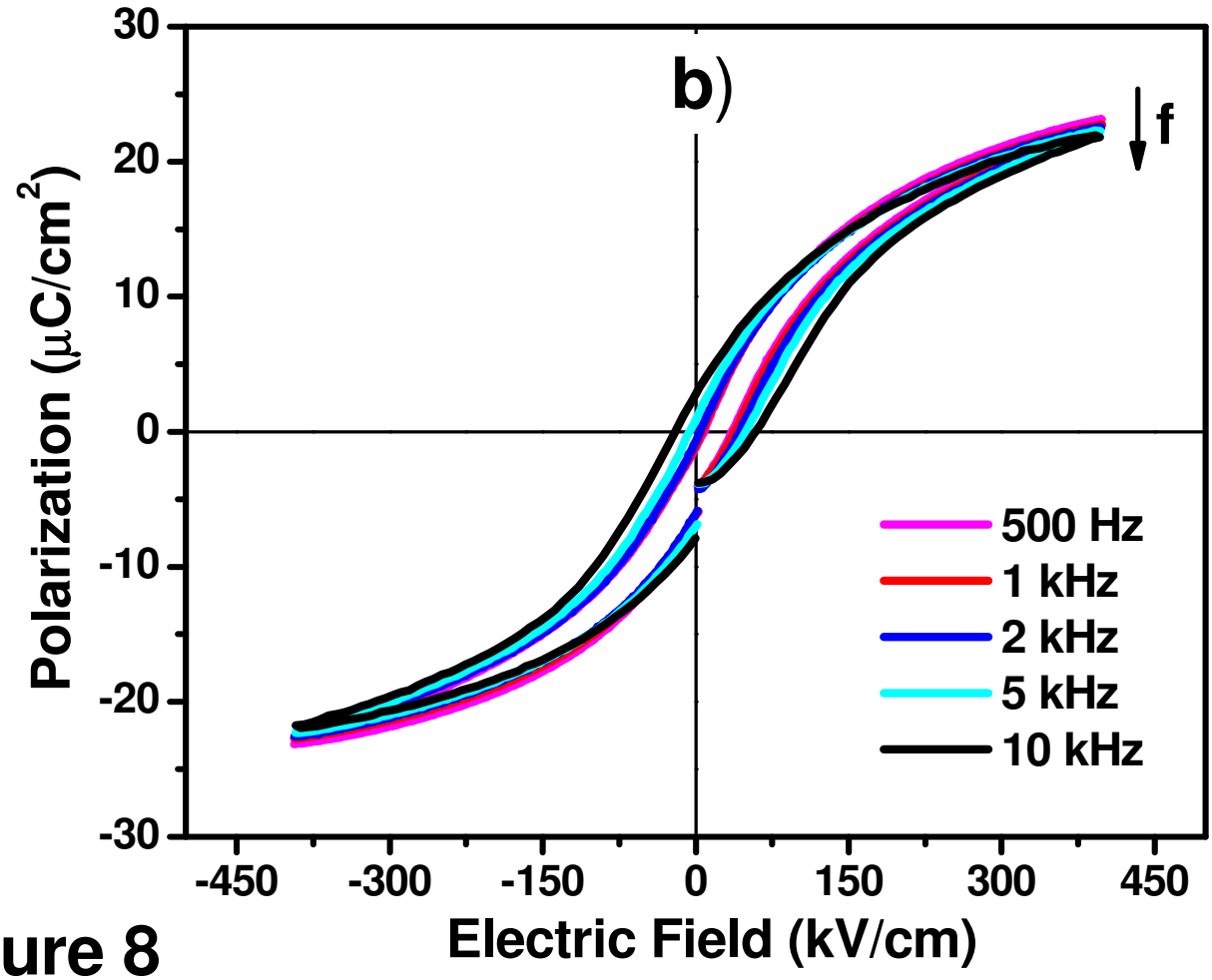
b)
f
Polarization (μC/cm²)
Electric Field (kV/cm)
500 Hz
1 kHz
2 kHz
5 kHz
10 kHz
30
20
10
0
-10
-20
-30
-450
-300
-150
0
150
300
450

Figure 8